Development 124, 1393-1403 (1997)
Printed in Great Britain © The Company of Biologists Limited 1997
DEV7520

Drosophila embryonic pattern repair: how embryos respond to *bicoid* dosage alteration

Ruria Namba†, Todd M. Pazdera†, Richelle L. Cerrone and Jonathan S. Minden*

Department of Biological Sciences and the Center for Light Microscope Imaging and Biotechnology, Carnegie Mellon University, Pittsburgh, PA 15213, USA

*Author of correspondence (e-mail: minden@andrew.cmu.edu)
†Contributed equally to the project and must be considered as first authors

SUMMARY

The product of the maternal effect gene, *bicoid* (*bcd*), is a transcription factor that acts in a concentration-dependent fashion to direct the establishment of anterior fates in the *Drosophila melanogaster* embryo. Embryos laid by mothers with fewer or greater than the normal two copies of *bcd* show initial alterations in the expression of the gap, segmentation and segment polarity genes, as well as changes in early morphological markers. In the absence of a fate map repair system, one would predict that these initial changes would result in drastic changes in the shape and size of larval and adult structures. However, these embryos develop into relatively normal larvae and adults. This indicates that there is plasticity in *Drosophila* embryonic development along the anterior-posterior axis. Embryos laid by mothers with six copies of *bcd* have reduced viability, indicating a threshold for repairing anterior-posterior mispatterning. We show that cell death plays a major role in correcting expanded regions of the fate map. There is a concomitant decrease of cell death in compressed regions of the fate map. We also show that compression of the fate map does not appear to be repaired by the induction of new cell divisions. In addition, some tissues are more sensitive to fate map compression than others.

Key words: cell death, compensation, *Drosophila*, pattern repair, *bicoid*

INTRODUCTION

Establishment and maintenance of proper proportions and pattern are of paramount importance in animal development. A great deal has been discovered about the molecular biology and genetics of pattern formation in developing organisms. Meanwhile, our understanding of pattern maintenance and repair is quite limited. Pattern repair is defined as the process of correcting a tissue that has been altered by either genetic or physical means to generate a normalized final pattern or structure. This process may be carried out by any combination of cell behaviors, such as cell division, fate alteration and cell death. Pattern repair, for the most part, has been studied by observing regeneration in surgically altered insect and amphibian limbs and insect imaginal discs (Bryant et al., 1981; French et al., 1976). Irradiation with X-rays, ultraviolet light and ligation have been used to examine pattern repair in developing insect embryos (Bownes, 1975; King and Bryant, 1982; Schubiger, 1976). In the sea urchin, embryonic regulation has been extensively studied by cell and tissue recombination experiments (reviewed in Davidson, 1989; Ettensohn et al., 1996). These studies demonstrated that these organisms have an impressive capacity for pattern repair, but shed little light on its molecular/genetic basis. In an effort to gain a molecular/genetic understanding of pattern repair, one needs an efficient and reproducible means to mispattern the organism as an alternative to surgically induced mispatterning.

Nüsslein-Volhard and co-workers recognized that embryos laid by females with varying doses of the anterior morphogen, *bicoid* (*bcd*), showed early mispatterning of anterior morphological markers. Females possessing one to six doses of *bcd* lay eggs that show a number of early developmental alterations; the cephalic furrow (CF), a transient cleft that demarcates anterior midgut and anterior head structures from the rest of the head, thorax and abdomen, is shifted anteriorly in reduced *bcd* embryos or posteriorly in increased *bcd* embryos (Frohnhöffer and Nüsslein-Volhard, 1986; Berleth et al., 1988; Driever and Nüsslein-Volhard, 1988). Other groups showed that the spacing and domains of expression of a variety of gap, segmentation and segment polarity genes is compressed in embryos laid by females with extra copies of *bcd* (Cohen and Jürgens, 1990; Eldon and Pirrotta, 1991; Struhl et al., 1989; Kraut and Levine, 1991). Mitotic domains, stereotypic clusters of cells that divide synchronously, of embryos derived from females with differing doses of *bcd* are expanded or compressed resulting in altered numbers of cells (Foe and Odell, 1989). Surprisingly, these embryos developed into normal, healthy adults (Frohnhöffer and Nüsslein-Volhard, 1986; Berleth et al., 1988). These observations indicate that the *Drosophila* embryo is capable of pattern repair and that embryogenesis is plastic. In order to gain a better understanding of these repair mechanisms, we have undertaken an analysis of how *bcd*-induced pattern defects are repaired as well as an in depth analysis of what defects may be occurring.

For brevity, we will refer to embryos laid by females with n doses of *bcd* as n*bcd* embryos. This nomenclature refers to the maternal genotype not the zygotic genotype of the animal.

To date, researchers of *bcd*-induced pattern changes have examined embryos from the time of egg deposition to gastrulation, as well as cuticle pattern at the end of embryogenesis (Busturia and Lawrence, 1994). Little is known about the events between gastrulation and cuticle secretion – the time when patterns are established and probably when pattern defects are repaired. Here we attempt to fill this gap.

MATERIALS AND METHODS

Fly strains

Oregon-R was used as a wild-type stock. 1*bcd* embryos were collected from *st ri bcd^{E1} roe p^{p}/TM3* mothers. Females carrying extra copies of the *bcd* gene were mostly derived from *BB9+16/CyO* (kindly provided by G. Struhl; Struhl, 1989). The *BB9+16* chromosome is a second chromosome derivative that carries two *P* elements which contain *bcd* genomic DNA inserts. A heterozygous balanced stock was used for the collection of 4*bcd* embryos. Homozygous *BB9+16* females were used to generate 6*bcd* embryos. *BB5+8/FM7* (stock T301 from the Tübingen Stock collection), which carries two *P[bcd]* inserts on the X chromosome, was used as an alternate source of extra copy *bcd* embryos.

Gross development

Dechorionated, precellularized embryos were lined up on a no.1 coverslip and covered with halocarbon oil. Transmitted light images of these embryos were taken with an inverted microscope (Olympus) fitted with a scientific-grade, cooled CCD camera (Photometrics) with a 20× objective lens every 30 minutes for 48 hours or until they hatched. In order to record the development of up to 20 embryos per session, the microscope was equipped with a programmable stage (Melles Griot) that repeatedly cycled between embryos. The electronic images were stored and processed on a UNIX workstation (Silicon Graphics) using Deltavision-Priism (Applied Precision) and in-house written software.

Cephalic furrow position measurement

Dechorionated, precellularized embryos were positioned on a coverslip dorsal side down. Transmitted light images of embryos within 10 minutes of CF formation were taken with either the aforementioned inverted microscope or a confocal microscope (MRC600, BioRad) using a 20× objective lens focused midway through the embryo. The position of the CF, expressed as percent egg length from the posterior, was calculated by determining the intersection of two lines connecting the anterior and posterior tips and the CF indentations.

Cuticle preparation

Overnight collections of embryos were dechorionated and allowed to develop for 22-24 hours to ensure the completion of cuticle secretion. Because of their slower development, 6*bcd* embryos were allowed to develop for 36-42 hours before their cuticles were isolated. All unhatched embryos and larvae were subjected to vigorous shaking in 1:1 heptane:methanol to remove their vitelline membranes. Devitellinized embryos were cleared according to the protocol of Lamka et al. (1992). The cuticles of at least 200 animals of each embryo-type were analyzed using phase-contrast or dark-field microscopy.

Salivary gland cell counts

Salivary glands were dissected from third instar larvae according to Rykowski et al. (1991). Fluorescence images of DAPI-stained salivary gland lobes using a 20× objective lens were recorded with a CCD camera.

Monitoring mitotic domains or cell death in vivo

To monitor cell divisions at the embryo surface in vivo, embryos were injected with either a solution of 0.25 mg/ml calcein or 1.5 mM RGPEG (Minden, 1996) into the intervitelline space according to the protocol reported by Minden et al. (1989). To visualize cell death, a solution of 0.25 mg/ml acridine orange in PBS was injected into the cytoplasm of syncytial embryos. Time-lapse recordings of laterally oriented embryos were initiated either at gastrulation for mitotic domain analysis or after the embryos developed to the germ-band-retraction stage, the time when cell death first is detectable. Each recording was composed of stacks of 6-8 optical sections, spaced 5 μm apart, taken at 1-5 minute intervals over a period of 8-12 hours. In order to analyze the cell death patterns over time in three dimensions, each image stack was projected into a single plane and the two-dimensional projections were viewed as a time-lapse series of images representing a 30-40 μm volume of the embryo.

Counting cell death figures in n*bcd* embryos

The number of dying cells was determined by counting acridine-orange-positive nuclei from projected image stacks taken 50 minutes apart to ensure that dying cells were not counted twice. Macrophages that had engulfed dying cells appeared as large cells containing multiple fluorescent bodies were not counted. Anterior cell death counting was confined to the region anterior to the CF in stage 11-12 embryos and, in post-stage 12 embryos, to the region anterior to the yolk including the gnathal segments. Epidermal cell death counting was restricted to the germband and excluded signal from the yolk and amnioserosa.

Antibody staining

Embryos were fixed and processed as described in Bomze and López (1994) using the following mouse monoclonal antibody dilutions; anti-INV undiluted to visualize ENGRAILED and INVECTED expression (Steve DiNardo), anti-AC 1:3 dilution (Sean Carroll) and anti-ELAV 1:1 dilution (Kalpana White). These antibodies were visualized with peroxidase-conjugated goat anti-mouse antibody (Vector Labs). A rat monoclonal anti-HB antibody (Paul McDonald) was used at a 1:500 dilution and detected with a goat anti-rat secondary antibody (Vector Labs). A rabbit polyclonal anti-EVE (Manfred Frasch) was used at a 1:4000 dilution and detected with a goat anti-rabbit secondary.

Calculation of brain volume

To determine the brain volume, fixed embryos of each class were incubated for 10 minutes in propidium iodide (20 μg/ml) and washed 3× 5 minutes in PBS. The fixation protocol used for antibody staining gave a propidium-iodide-staining pattern that highlighted a ring of the cytoplasm and weakly stained the nucleus. Image stacks of propidium-iodide-stained embryos were collected using a 60× objective lens on a confocal microscope (MRC 600, BioRad). Serial sections 1 μm apart were obtained from the embryo surface through the supraoesophageal ganglia for one side of the embryo. The areas of the brain in each section was determined and summed to obtain a volume. The cell density in random sections from each class of embryos was determined by counting the number of cells in an area of 750 μm^2 of brain.

Isolation of *rpr* cDNA

A cDNA clone of *rpr* was isolated by RT PCR of third instar larval RNA with the following primers: CGCGAATTCATTGACTTT-TTGTTTGAC and CCGGAATTCTGAATAAGAGAGACACC (White et al., 1994).

Table 1. Compilation of viability and morphometry data for n*bcd* embryos

Embryo-type	Viability to adult (%)	Cephalic furrow position (%EL)	Brain volume ($\times 10^3$ μm^3)	Brain density (cells/775 μm^2)	Salivary gland size (cells/lobe)
1*bcd*	79	73.3±0.9	40.2±3.7	nd	121±9.9
2*bcd*	79	67.4±1.4	40.0±3.2	36.0±3.6	141±13.2
4*bcd*	80	59.0±1.5	nd	nd	151±8.7
6*bcd*	32	53.9±1.5	38.7±4.6	35.4±4.3	155±9.8

EL, egg length; nd, not determined

In situ hybridization

The *rpr* and S59 cDNAs (a gift of Manfred Frasch; Dohrmann et al., 1990) were gel isolated and labeled with digoxigenin-dUTP (Boehringer-Mannheim) by extension of random hexamers with DNA polymerase I Klenow fragment. Embryos were processed as whole mounts as described (Tautz and Pfeifle, 1989). Complexed probe and RNA was detected using an alkaline-phosphatase-conjugated antibody against the digoxigenin dUTP (Boehringer-Mannheim).

Classification of phenotypes

Three general classes of phenotype were defined to indicate the severity of defects caused by altered *bcd* dosage: (1) wild-type, where there were no obvious changes seen at the stated level of resolution of the experiment; (2) mild, where only a partial loss or fusion of cells was seen in a few segments and (3) severe, where more than three segments were malformed. The severe class often included embryos with defects throughout the embryo.

RESULTS

Survival of n*bcd* embryos and time-lapse analysis of development

Embryos endowed with one to four doses of *bcd* mRNA survived to adulthood with a high frequency (80%, see Table 1). In contrast, only 50% of the embryos generated by 6*bcd* females hatched into larvae and 60% of the surviving larvae eclosed as adults – giving an overall survival rate of 30%. Time-lapse microscopy of 6*bcd* embryos showed that 53% failed to hatch (n=57). The CF of the 6*bcd* embryos was displaced posteriorly compared to that of the 4*bcd* embryos and the clypeolabrum was significantly larger. After stage 12, clusters of free floating cells were often seen in the intervitelline space around the clypeolabrum in 6*bcd* embryos, but were rarely seen in wild-type embryos (Fig. 1A). These clusters of cells are believed to be dead cells and macrophages.

The embryos that failed to hatch were divided into five phenotypes (Fig. 1B-E). Class 1 embryos, 37% of unhatched embryos, first appeared abnormal during head involution, stage 14. The clypeolabrum started to retract but the dorsal ridge was not able to envelop the tip of the enlarged clypeolabrum to complete the head involution process. This often created a large mass anterior to the dorsal ridge constriction. In those embryos that managed to reach stage 17, the two mouth hooks were separated from one another by the excess head tissue pushing between them (compare the class 3 embryo in Fig. 1C to class 1 6*bcd* embryo in Fig. 1B). Most embryos, however, did not reach stage 17 due to secondary abnormalities that affected posterior development. Class 2 embryos, 27% of unhatched embryos, had yolk leakage outside the gut into the head cavity (Fig. 1D) or intervitelline space. The yolk breaches mostly occurred at, or after, the completion of germband retraction, stage 12–13, and were occasionally seen as late as gut constriction in stage 15. The cause of the 'yolk displacement' phenotype could possibly be compression of the abdominal fate map leading to failure of dorsal closure and/or gut development. This phenotype was observed in many class 1 (head involution defective) embryos after the failure of clypeolabrum retraction. Except for the site where the yolk leakage occurred, the development of the rest of the body appeared to proceed on schedule but with obvious abnormalities. Class 3, 17% of unhatched embryos, developed normally up to stage 17 (Fig. 1C). Class 4 and 5 each occupied 10% of the unhatched embryos. The development of class 4 embryos ceased before completing germband retraction in stage 12. These embryos developed a large void in

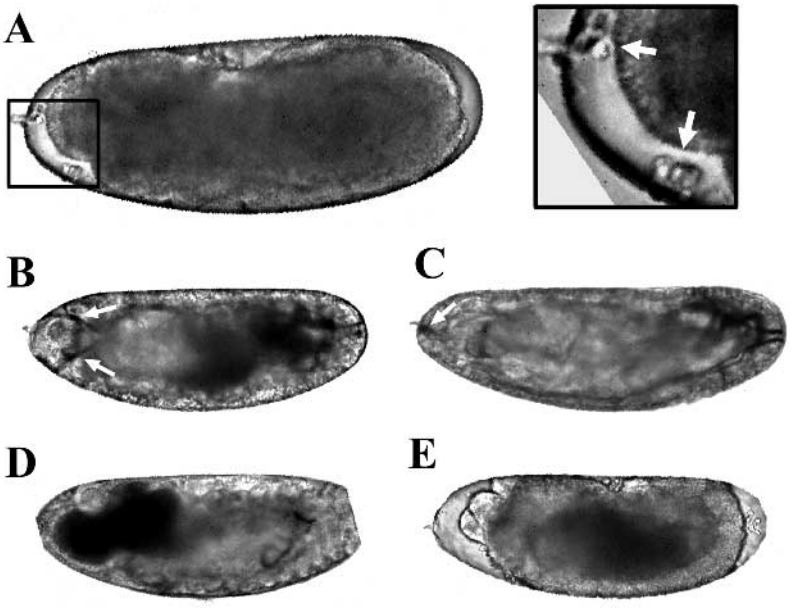

Fig. 1. Time-lapse analysis of 6*bcd* embryos. Shown here are selected images of transmitted light time-lapse recordings of 6*bcd* embryos. (A) A stage 12 embryo that eventually hatched and a magnified view of cell clusters (white arrows) in the anterior intervitelline space is shown on the right. (B) A class 1 embryo at stage 17. Excess tissue is present between mouth hooks (arrows). (C) A class 3 embryo at stage 17. This embryo had no obvious defects but did not hatch. (D) A class 2 embryo where the yolk has leaked into the anterior head cavity. The abdominal half of the embryo developed normally. (E) A class 4 embryo at the end of the germ-band stage. Notice the large intervitelline space containing clusters of dead cells and macrophages.

the anterior intervitelline space that contained a massive amount of dead cells (Fig. 1E). Class 5 embryos showed unsynchronized cellularization (data not shown).

In order to determine the correlation between viability and CF position, the CF position was determined for live 6*bcd* embryos, which were then allowed to develop for a total of 48 hours and then scored for hatching. The average CF position for 6*bcd* embryos was 53.9±1.5% egg length (EL) relative to the posterior tip (Table 1). Embryos that formed the CF more posterior to the mean position died at almost twice the frequency (18/29) of the population of embryos that formed the CF anterior to the mean position (11/33). The mean CF position of the embryos that failed to hatch was 53.4% EL, compared to 54.1% EL for the survivors. These results demonstrate that embryonic lethality correlates to the extent of mispatterning, the more posteriorly shifted the CF, the lower the probability of survival.

To eliminate the possiblility that the 6*bcd* defects were the result of genetic background effects resulting from homozygous *BB9+16* mothers, we assayed the viability and CF position of 6*bcd* embryos laid by *BB5+8;BB9+16* *trans*heterozygous females mated to wild-type males. The CF position of the *trans*heterozygous 6*bcd* embryos was 55.5% EL. This was intermediate between 59.0% EL for *BB9+16/CyO* 4*bcd* embryos and 53.9% EL for *BB9+16/BB9+16* 6*bcd* embryos. The difference in CF position in 6*bcd* embryos laid by the different females is most likely due to variation of *bcd* expression depending on the chromosomal location of the various *P [bcd]* elements. The hatching rate of *trans*heterozygous 6*bcd* embryos was 81%, compared to 50% for *BB9+16/BB9+16* 6*bcd* embryos and 90% for *BB9+16/CyO* 4*bcd* embryos. The mean CF position of the *trans*heterozygous 6*bcd* embryos that failed to hatch was 53.1% EL as compared to 55.8 % EL for the survivors. This is very similar to the mean CF position of the failed *BB9+16* homozygous embryos. The majority of unhatched *trans*heterozygous 6*bcd* embryos displayed class 1 head involution defects. These data support the observation that the more posteriorly shifted the CF, the lower the embryonic survival. In addition, the two sources of 6*bcd* embryos produced similar phenotypes of embryonic lethality indicating that the observed phenotypes were dependent on *bcd* dosage and not on the genetic background of the stocks.

Cuticular defects in n*bcd* embryos

Wild-type and 1*bcd* animals developed normal cuticles, while 15% of the 4*bcd* animals had one missing or a pair of fused denticle belts (Fig. 2A). The most severely affected were the 6*bcd* embryos and larvae. 30% of 6*bcd* embryos and larvae had normal cuticular structures (Fig. 2B), while the rest were abnormal. Denticle abnormalities ranged from embryos with mild defects that had missing or fused abdominal denticle belts (25%, Fig. 2C), to severe defects that either failed to develop any visible cuticle segmentation (24%) or had grossly

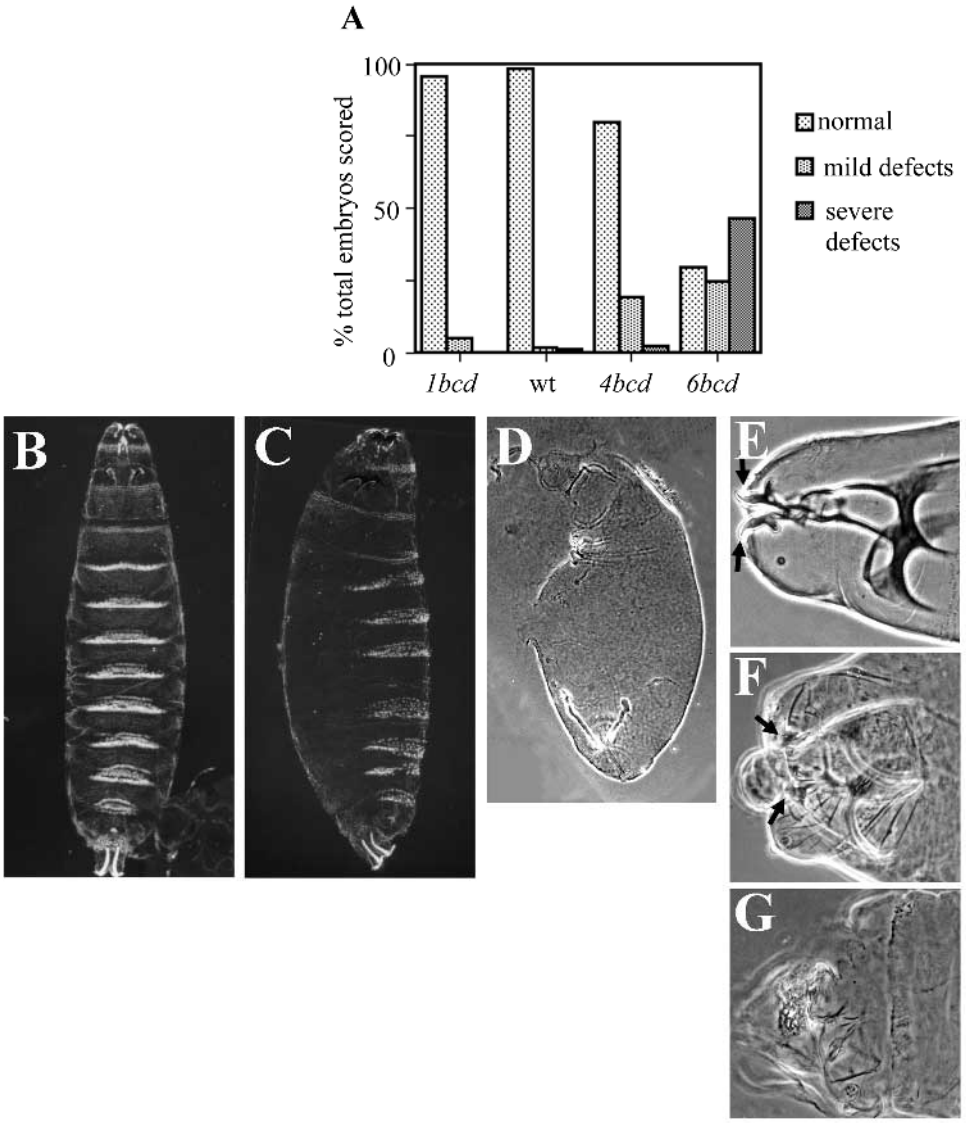

Fig. 2. Cuticle analysis of n*bcd* embryos**.** (A) A bar graph of the distribution of denticle belt defects of n*bcd* embryos. (B-D) Cuticle preparations of 6*bcd* embryos ranging from normal (B), mild (C) and severe (D) – anterior up. Notice the fusion of T3 and A1 and deletion of A4 in C. The embryo in D is missing denticle belts and head structures. (E-G) Head structures of 6*bcd* embryos ranging from normal (E), mild (F) and severe (G) – anterior to the left. The embryo in F has abnormal head structures resulting from incomplete head involution. Notice a sac between two mouth hooks (arrows). The embryo in G is missing all head structures except some pigmentation, leaving a hole at the anterior end. B and C are dark-field micrographs and D-G are phase-contrast micrographs.

malformed denticles affecting more than two segments (21%, Fig. 2D). The denticle fusions and deletions generally occurred between the third and fourth abdominal segments for 4*bcd* and 6*bcd* embryos and larvae. Analysis of third instar 6*bcd* larvae showed that animals with fused or missing denticles had reduced viability relative to normal animals, as the proportion of defective animals decreased with each molt (data not shown).

There appeared to be a dramatic increase in mouth part defects between 4*bcd* embryos and 6*bcd* embryos. The mouth parts of 55% 6*bcd* animals formed aberrantly. A minority (13%) of the abnormalities had well-formed mouth parts that were positioned improperly (Figs 1B, 2F). The rest had abnormal or missing mouth structures (Fig. 2G). Some embryos completely lacked mouth structures leaving a large hole in the head cuticle, which is consistent with the head involution defects seen in the time-lapse recordings.

Cell number variation of brain and salivary glands in n*bcd* embryos

In an effort to determine if altered *bcd* doses perturbed internal-anterior structures, we measured brain volume and cell density and cells per salivary gland (Table 1). In all cases, the size of the brain was constant at approximately 40×10^3 μm^3. The number of brain cells per unit area was also independent of *bcd* dosage; 35.5 cells/750 μm^2 area. This indicated that either the size of the brain anlage was not affected by *bcd*-induced mis-patterning or the altered brain was compensated for during subsequent brain development.

The number of cells per salivary gland was determined for third instar larvae since the cell number is fixed at the end of embryogenesis and the glands are much easier to dissect at this stage (Table 1). 2*bcd* embryos had an average of 141 cells per salivary gland lobe. There was less than one standard deviation increase in cell number for 4*bcd* animals, while 4*bcd* and 6*bcd* counts were nearly identical. Larvae from 1*bcd* mothers had salivary glands that were significantly reduced in cell number from wild type. These data indicate that there is an upper limit to the salivary gland cell number and that expanded regions can be regulated toward normal cell counts for those embryos that survive to third instar larvae. Conversely, compressed salivary gland anlagen do not appear to be regulated and cannot increase cell number to match wild type.

Mitotic domain changes in 6*bcd* embryos

To determine changes in the mitotic patterns of n*bcd* embryos, fluorescent dye was injected into the intervitelline space of embryos during cellularization. The fluorescent dye occupies the spaces in between cells showing a bas relief of the embryo surface (Warn and McGrath, 1986; Kam et al., 1991). When a cell at the surface of the embryo enters mitosis, it rises out of the surface of the epithelium and can be seen as a round void surrounded by a fluorescent ring. The overall shape and order of appearance of the mitotic domains was unchanged in the 6*bcd* embryos that eventually hatched and those of classes 1-3 (Fig. 3). The size of the anterior mitotic domains were significantly enlarged, but there were no signs of mitotic silencing in the anterior or extra mitoses in the posterior of these embryos (data not shown).

Apoptosis in embryos with varying doses of *bcd*

The observation of the intervitelline cell clusters and the normalization of salivary gland size led to the suspicion that cell death played a role in repairing expanded regions of the fate map. Two approaches were taken to investigate changes in cell death patterns in n*bcd* embryos. First, time-lapse recordings of embryos injected with the vital dye acridine orange (AO) were used to determine the dynamics of cell death. Second, cells fated to be eliminated by apoptosis were visualized by in situ hybridization of *reaper* (*rpr*) mRNA (White et al., 1994). Three-dimensional, time-lapse recordings were made of 1*bcd*, 2*bcd*, 4*bcd* and 6*bcd* embryos. The fluorescent signal from a dying cell persisted for 30-40 minutes. The engulfment of dead cells by macrophages confused the time-lapse interpretation because the AO signal from the ingested dead cells persisted presumably because the macrophages were continually engulfing dead cells. In order to assess the cell death patterns, careful analysis of the location and time of a cell's demise had to be discerned from a background of fast moving, highly fluorescent macrophages. Fig. 4 shows images taken from a time-lapse recording of AO injected embryos. At least four time-lapse recordings were made of 1*bcd*, 2*bcd* and 6*bcd* embryos. The 6*bcd* embryos used for this analysis did not exhibit either head involution or yolk displacement defects and all hatched. The average number of dying cells seen at 50 minute intervals was determined for the head and abdomen of n*bcd* embryos (Fig. 4D). This ensured that all non-marcophage signal originated from newly dying cells that

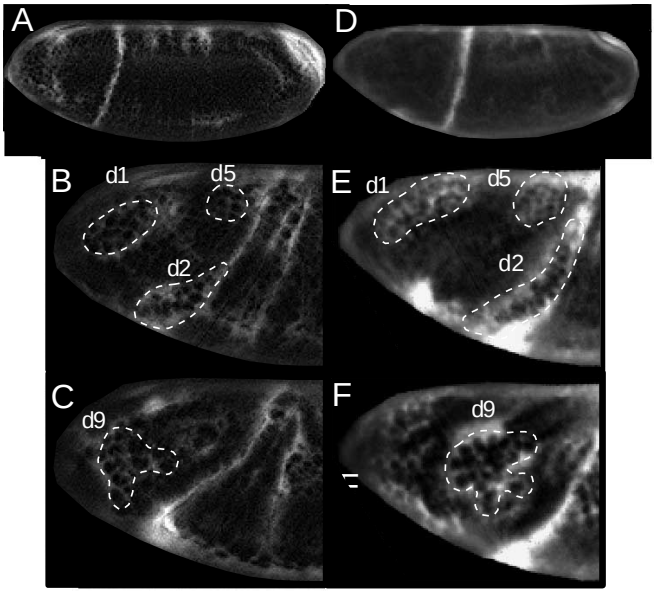

Fig. 3. Anterior mitotic domains revealed by intervitelline injection of RGPEG. Selected images from time-lapse recordings of a wild-type (A-C) and a 6*bcd* (D-F) embryo. Intervitelline dye injection reveals morphogenetic folds and mitoses at the surface of the embryo. Mitoses appear as dark circles surrounded by a brightly fluorescent ring. (A,D) Full lateral view of CF formation; (B,E) magnified views of anterior half of a embryo highlighting mitotic domains 1, 2 and 5 taken 21 and 15 minutes after the previous image, respectively; (C,F) similarly magnified views highlighting mitotic domain 9 taken 21 and 18 minutes after the previous image, respectively. The mitotic domains are highlighted by a white dashed line. Anterior mitotic pattern does not change in a 6*bcd* embryo but each anterior mitotic domain of a 6*bcd* embryo is larger than that of a wild type.

were not counted in the previous time point. 6*bcd* embryos laid by *BB9+16* or *BB5+8* homozygous females exhibited the same changes in the cell death pattern. These results show a direct relationship between the amount of cell death and the expanded region of the embryo – there is an increase in cell death in the expanded head domains of 6*bcd* embryos and expanded trunks of 1*bcd* embryos. Conversely, compressed regions of the embryo appeared to have less apoptosis.

The time-lapse recordings of 6*bcd* embryos showed that the embryonic brain (which is visible due to the background fluorescence) first appeared enlarged relative to wild-type embryos but, over time, one could see macrophages hovering over the surface of the brain as it gradually decreased to normal size. There was also increased cell death in the clypeolabrum, which is believed to be the source of the perivitelline cell clusters. The cell clusters are a mixture of dead cells and macrophages as evidenced by their AO staining and, in some cases, motile behavior.

To corroborate the in vivo AO observations, embryos with different *bcd* doses were fixed and stained for *rpr* expression. 6*bcd* embryos at late stage 11 had clear increases in *rpr* expression in the expanded head domains and a corresponding decrease in *rpr* expression in their abdominal domains (Fig. 5).

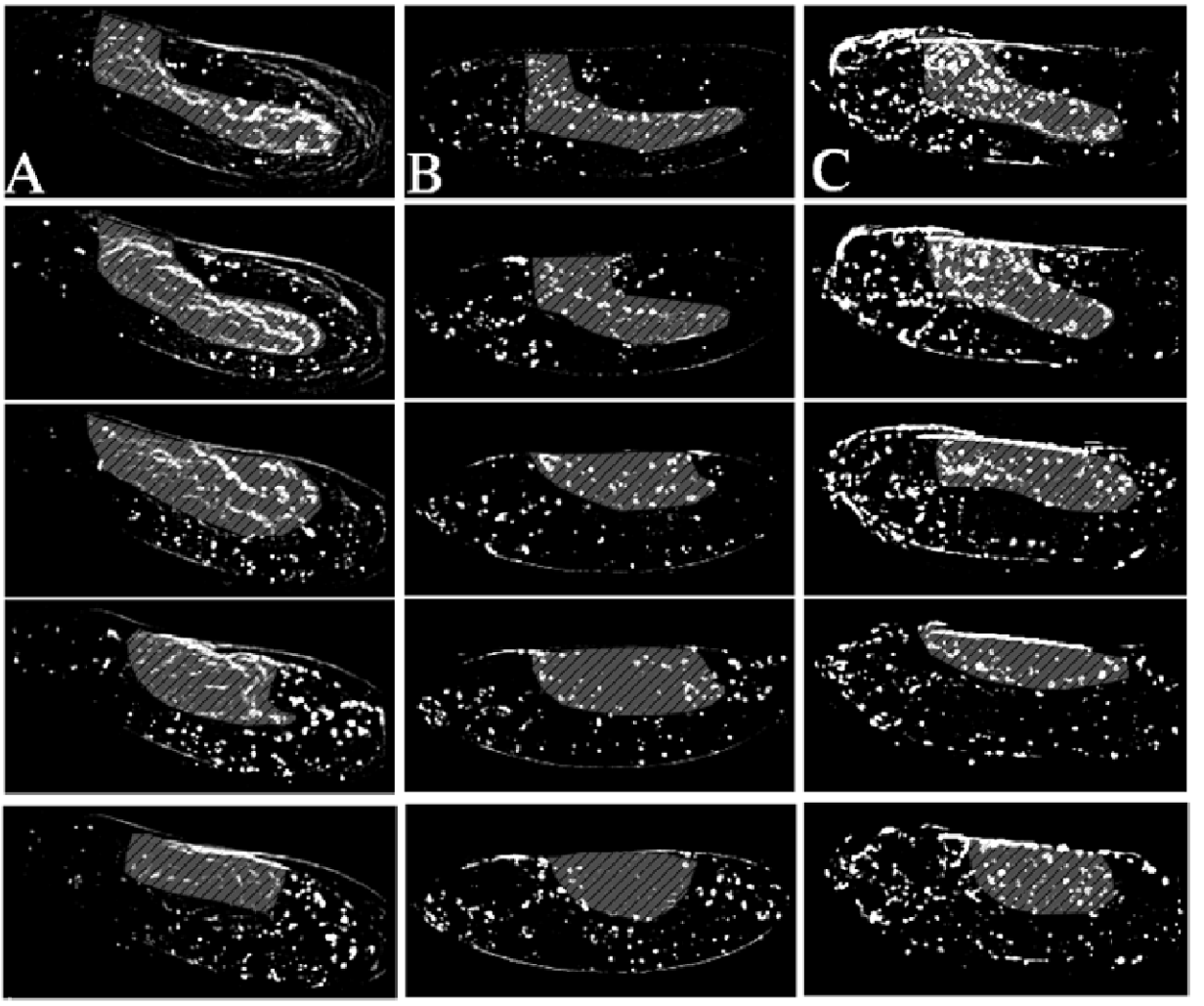

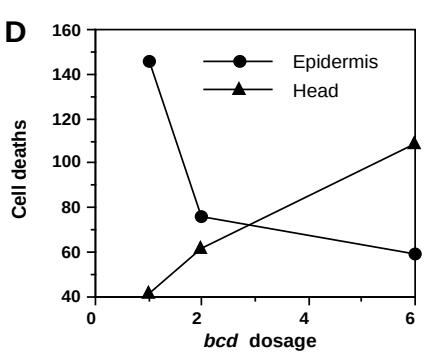

Fig 4. Cell death analysis of n*bcd* embryos. To reveal cell death, embryos were injected with AO. Selected time points were taken from time-lapse recordings of cell death in 1*bcd* (column A), 2*bcd* (column B) and 6*bcd* (column C) embryos. Equivalent staged embryos from each class are shown from late stage 11 (top) through early stage 14 (bottom). Each image is a contrast-enhanced projection of eight 5 μm optical sections, which were individually background subtracted. Each image stack contains optical information from the surface of the embryo to a depth of 40 μm into the laterally mounted embryo. This represents approximately 50% of the dorsal-lateral volume of the embryo. The dying cells appear as small white punctate spots. Macrophages are larger than the dying cells and are the source of the fluorescence around the yolk. The yolk region is indicated by hatching. The number of AO-positive dying cells increases in expanded regions and decreases in compressed regions of the developing embryo. (D) A graph of the average number of dying cells in the epidermis and head taken from time-lapse recordings similar to those in A-C. Cell counts were restricted to the germ band for the abdominal counts and to the anterior of the yolk and CF for the head. Large diffusely staining macrophage were not counted.

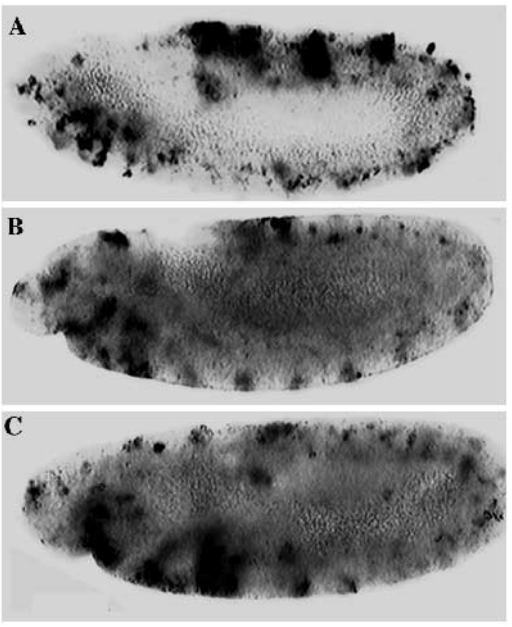

Fig. 5. *reaper* expression in n*bcd* early stage 12 embryos. (A) A lateral view of a 1*bcd* embryo; (B) *rpr* expression in a wild-type embryo; (C) *rpr* expression in a 6*bcd* embryo. Notice the increasing *rpr* expression in the head and the decreasing *rpr* expression in the abdomen moving from A-C.

Similarly, in 1*bcd* embryos *rpr* expression was increased in the abdomen and decreased in the head. These results indicate that many of the excess cells in expanded regions are destined to be eliminated by cell death.

Effect of fate map compression on *engrailed* (*en*) expression in the epidermis and central nervous system

In order to determine if fate map compression led to segmental defects in all tissues, a number of molecular probes were used to assess the formation of epidermal, mesodermal, central nervous system (CNS), and peripheral nervous system (PNS) cell types.

ENGRAILED (EN) is expressed both in the early epidermis and CNS (DiNardo et al., 1985). Anti-EN antibody staining revealed that approximately 10% of 4*bcd* embryos between stages 12 and 15 had defects in the epidermal segments, but none in the CNS (Fig. 6). Defects included fusions or deletions of EN stripes. The remaining embryos appeared normal in both the CNS and epidermal stripes.

6*bcd* embryos between stages 12 and 15 were divided into three classes. 38% of the embryos had severe defects in EN pattern where the CNS clusters and epidermal stripes were either fused, missing or displaced. 30% of the embryos had defects only in the epidermis without a corresponding defect in the neural clusters of the ventral nerve cord. 32% of the embryos appeared normal in both the CNS and epidermal stripes (Fig. 6 and Table 2). There were no instances of embryos with defects in the CNS and not in the epidermis.

Embryos were probed with anti-ELAV antibody, which recognizes postmitotic neurons (Robinow and White, 1991). Approximately 94% of 4*bcd* and 1*bcd* embryos had wild-type numbers of peripheral neurons arranged in a normal pattern. No fusions were seen between clusters of peripheral neurons nor were there deletions of neuronal clusters. Approximately 50% of the embryos laid by 6*bcd* mothers had defects in their peripheral neurons, which could be seen as early as stage 12 when the antibody first recognizes some neurons. In many

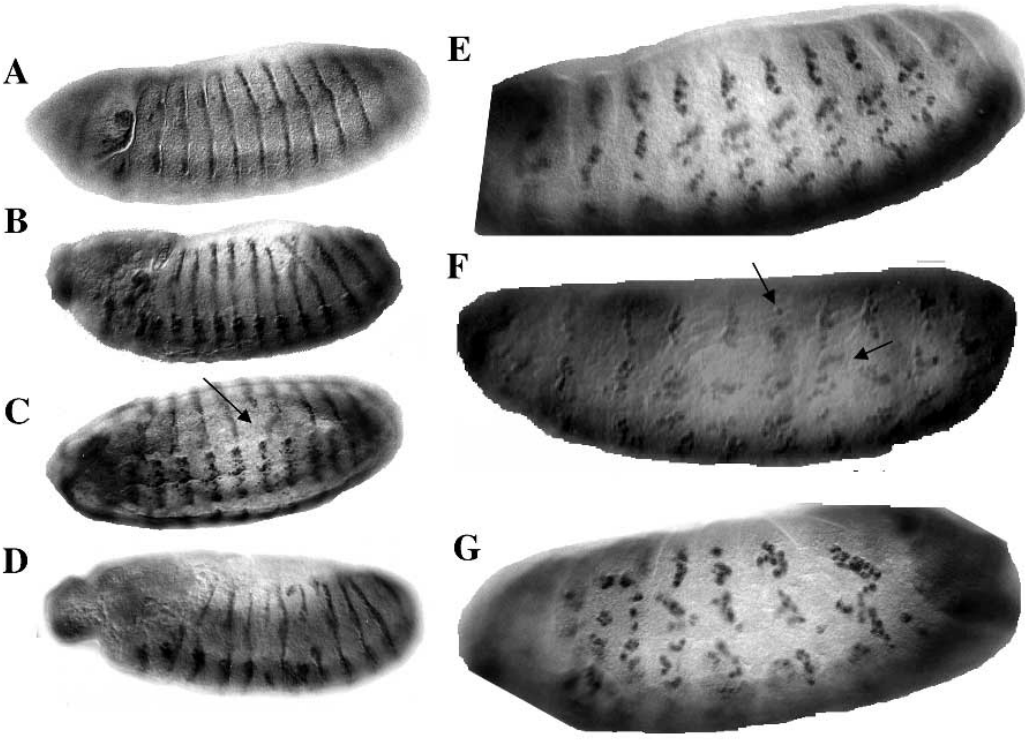

Fig. 6. Compression defects in 6*bcd* embryos as revealed by EN and ELAV protein distribution. (A-D) Stained for EN protein expression. (A) a wild-type embryo; (B) a 4*bcd* embryo with a dorsal epidermis fusion; (C,D) two 6*bcd* embryos with mild and severe defects, respectively. The arrow in C points to a loss of EN cells in one segment and a fusion with an adjacent segment without affecting the CNS pattern. (E-G) Compression defects in the late peripheral nervous system of 6*bcd* embryos labeled with anti-ELAV antibody. (E) a 2*bcd* embryo; (F) a 6*bcd* embryo with mild defects. Notice the absence of a few neurons in one abdominal segment (left arrow) and a few ectopic neurons in an adjacent segment (right arrow). (G) A 6*bcd* embryo with severe defects.

Table 2. Compilation of defects seen in 6*bcd* embryos

Defect severity (%)	EVE stage 5-8 *n*=23	AC stage 8-11 proneural clusters *n*=27	EN stage 8-10 epidermis *n*=45	HB stage 11-13 PNS neuroblast *n*=56	ELAV stage 13-15 PNS neurons *n*=45	EN stage 12-15 CNS neurons *n*=100	EN stage 12-15 epidermis *n*=100	EVE stage 15 dorsal mesoderm *n*=45	S59 stage 12-15 somatic mesoderm *n*=811	cuticle >stage 17 *n*=234
normal	87	76	91	46	49	62	32	31	44	30
mild	0	0	0	23	23	0	30	44	25	25
severe	13	24	9	30	28	38	38	25	31	45

st., stage; normal, similar to wild-type embryos; mild, one or two affected segments; severe, more than two perturbed segments.

embryos, the neurons were dramatically displaced (Fig. 6). The remaining 50% of the 6*bcd* embryos appeared normal. The number of neurons in each segment was equivalent to wild-type and there were no fusions between adjacent clusters. Normal embryos were found at all stages of development. Thus, as seen with EN expression, the PNS and CNS are less affected by increased *bcd* dosage than the epidermis.

Effect of fate map compression on neuroblast and neuron formation

The CNS could prevent or repair fate map compression defects by two general schemes; either ensure the proper formation of neuroblasts during neuroectoderm fate selection or compensate for the initial reduction in neuroblast formation by allowing the neuroblasts to produce more progeny neurons. To discriminate between these two alternatives, embryos from each genotype were stained with an antibody against ACHAETE (AC), which transiently labels all S1 CNS neuroblasts in stage 8-11 embryos (Skeath and Carroll, 1992). Embryos were also stained with a HB antibody which transiently labels all neuroblasts (Tautz et al., 1987). Despite the obvious anterior expansion and posterior compression, the relative numbers of AC-staining S1 neuroblasts appeared to be equivalent in 76% of 6*bcd* when compared to 2*bcd* embryos (Table 2). The remaining 6*bcd* embryos exhibited defects where several segments had missing or disorganized neuroblasts. Examination of CNS neuroblasts stained with HB gave similar results. HB-stained embryos were examined for peripheral neuroblast defects in stage 11-13 embryos. In spite of the size variation in the gnathal buds of n*bcd* embryos, approximately 4-6 neuroblasts were labeled in the gnathal segments in embryos from each class. The number of peripheral abdominal neuroblasts were equivalent in 1*bcd*, 2*bcd*, 4*bcd* and approximately 50% of 6*bcd* embryos at stage 11. The remaining 50% of the 6*bcd* embryos were split between those with mild and severe defects. Those with severe defects were missing numerous abdominal neuroblasts and often had obvious head expansion defects (Table 2). These results indicate that the number of cells allocated to become neuroblasts are equivalent among each of the 1, 2 and 4*bcd* genotypes and 50% of the 6*bcd* embryos. These 6*bcd* embryos with normal neuroblast formation probably represent a majority of those that continue on to hatch.

Effect of fate map compression on mesoderm formation

Somatic mesodermal precursors during stages 12-15 were

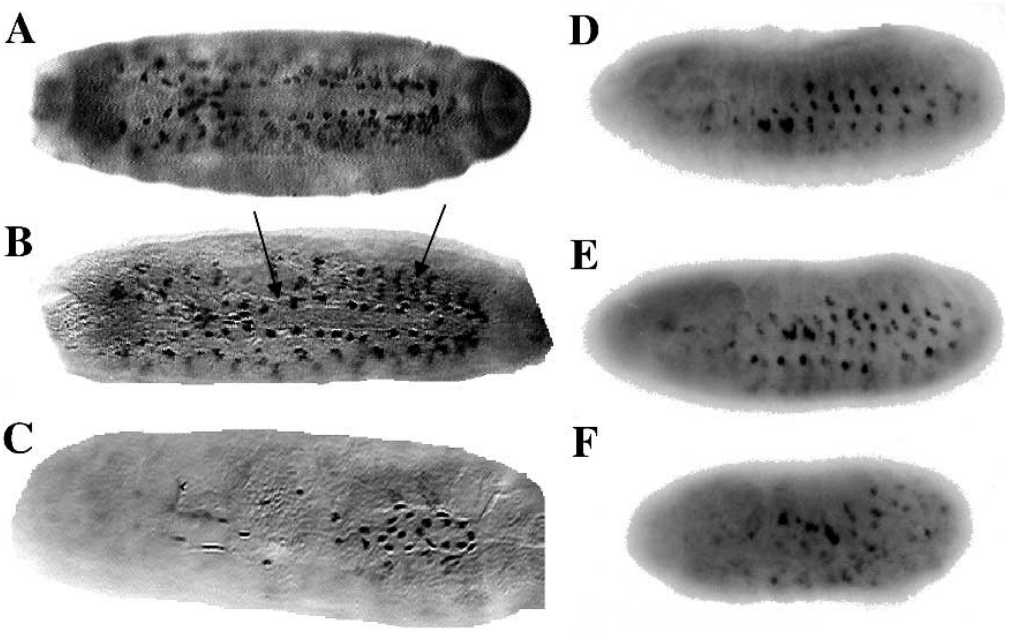

Fig. 7. Analysis of the dorsal vessel and somatic mesoderm in n*bcd* embryos. To assess dorsal vessel formation embryos were fixed at late stage 15 and stained with anti-EVE antibody (A-C). (A) A 2*bcd* embryo; (B) a mildly affected 6*bcd* embryo. The left arrow indicates the loss of an EVE-expressing cell. The right arrow indicates a cluster of ectopic cells. (C) An embryo with severe defects in the dorsal vessel. Notice that there is almost a complete loss of the anterior cells and a clustering of the posterior cells. Somatic mesoderm formation was analyzed by in situ hybridization with a S59 probe (D-F). (D) A 4*bcd* embryo at stage 12; (E) a 6*bcd* embryo with mild defects. The most ventral row of S59-expressing cells belong to the CNS. Notice that A4 is missing a CNS cluster and a spatial organization of three mesodermal clusters is abnormal. A7 only has two mesodermal clusters. (F) A 6*bcd* embryo with severe defects. Notice that the normal spatial organization of S59-expressing cells is lost in almost all the segments.

probed for S59 mRNA expression (Dohrmann et al., 1990). More than 80% of 4*bcd* were completely normal with respect to cluster size and position within each hemisegment. Increasing the *bcd* dosage to six reduced the fraction of embryos with a normal S59 pattern to 44%. The remainder were split between mild defects (25%) with one or two abnormal segments, and severe defects (31%), which often affected throughout the embryo (Fig. 7, Table 2).

The dorsal vessel, which gives rise to the larval heart, is derived from dorsally migrating mesodermal cells. A subset of these cells express *eve* (Frasch et al., 1987). Stage 15 embryos derived from n*bcd* females were immunostained for EVE. 1*bcd* embryos showed wild-type numbers of EVE-expressing dorsal mesoderm cells. 31% of 6*bcd* embryos had normally patterned dorsal mesoderm cells. 44% of the 6*bcd* embryos had mild defects where only a few cells were deleted or displaced. The remaining 25% had severe defects often missing the anterior *eve*-expressing cells and a severe compression of posterior cells (Fig. 7; Table 2). As seen with the nervous system markers, the mesoderm was less perturbed by increased *bcd* dosage than the epidermis. This result also indicates that the *eve*-expressing mesoderm cells are more affected than the somatic muscles.

DISCUSSION

Phenotypes of n*bcd* embryos

Two major phenotypes were observed in the non-hatching 6*bcd* embryos: failure of head involution and a yolk leakage defect. The head involution failure appeared to be due to the excess of anterior tissue that could not be properly internalized. The excess of anterior tissue demonstrates an upper threshold for the number of cells that can be eliminated by programmed cell death in expanded regions. The yolk displacement phenotype may be the result of either posterior compression or anterior expansion. In some yolk-displaced embryos, the yolk leaked directly into the intervitelline space – indicating a breach in the epidermis, while in others the displaced yolk was contained within the epidermal sheath – indicating failure of gut formation. Some embryos displayed both head involution and yolk displacement defects. Our data indicate that the 6*bcd*-induced lethality is directly related to the extent of mispatterning. The absence of these phenotypes in 1*bcd* or 4*bcd* embryos demonstrates that this level of mispatterning did not exceed the limits of pattern repair for either compressed or expanded regions of the fate map.

There is a graded increase of abdominal denticle fusions and deletions with increasing doses of maternal *bcd*. These defects mostly affected segments A3 and A4. A possible explanation for the localized defects is that these embryos have a mostly normal posterior domain, while the anterior domain is expanded. The anterior expansion is graded, where the extent of expansion is greatest at the anterior tip and decreases toward the middle of the embryo (Foe and Odell, 1989). This causes the compression to be most severe near the middle of the embryo, where segments A3 and A4 arise. Nearly one-third of all 6*bcd* embryos have fused or deleted denticle belts. The defects are not limited to gross denticle mispatterning. Nearly 80% of the 6*bcd* embryos that hatch as first instar larvae have mild denticle defects that include denticle hair deletions and polarity errors (data not shown). The cuticle and mitotic domain results, and those of Bustaria and Lawrence (1994), show that the epidermis cannot increase cell number in response to a mispatterning event that reduces the cell number. The observation that cell number cannot be increased in the epidermis can be extended to include the salivary gland in 1*bcd* animals. The embryonic brain, however, does not show a reduction in size or cell density in 1*bcd* embryos. This indicates that different tissues may have different minimum cell number thresholds.

Chronology of compression defects: does compression repair occur?

The abdomen of 6*bcd* embryos is compressed. We see that the majority of these embryos develop abnormally. When and where do these defects occur? 90% of 6*bcd* embryos develop to gastrulation where one observes the normal number of *eve* and *en* stripes, albeit the stripes are closer together. Postgastrulation mitoses appear to be normal as revealed by intervitelline injection of fluorescent dyes and anti-tubulin staining (Foe and Odell, 1989). Proneural patterning at stages 8 and 9 was 75% normal. By stages 11-13, the number of peripheral neuronal defects increased to 50%. The CNS at stage 12-15 was somewhat less affected than PNS at 62% normal. At the same stage, only 32% of 6*bcd* embryos had normal epidermal patterns. There were also reductions in cell numbers in the mesoderm at stage 15 where more dorsal mesoderm structures were slightly more affected. These data are in agreement with those of Maggert et al. (1995) who have shown that reducing the width of the mesodermal stripe leads to the loss of visceral mesoderm and cardiac precursors.

These results show that compression defects are not corrected and that reducing the number of cells below a minimum threshold of cells fated to particular structure leads to structural defects. The susceptibility to compression defects can be explained by the order of cell type specification. The mesoderm is the first group of cells to segregate from the epithelial monolayer. The number of mesodermal cells per segment is controlled by the width of the stripe of invaginating mesoderm and segmental width. Next, the CNS neuroblasts delaminate; followed by the PNS neuroblasts, or mother cells. Each of these segregation events reduce the number of potential epidermal cells. Thus, if the initial number of cells per segment is limited by fate map compression, it seems reasonable that the epidermis would be most affected, followed by PNS, and then CNS.

6*bcd* embryos that had head involution or yolk displacement defects generally had abdominal defects affecting all three germ layers in three or more segments. We believe these massive defects indicate a system-wide failure where too many segments were compressed below a certain threshold and cells that normally do not signal each other begin to interact, causing a breakdown in the overall signaling network. The severity of defects seen in 6*bcd* embryos probably depends on the combined effects of embryo length, cell density and the absolute amount of BCD protein. These factors result in the observed distribution of phenotypes. A precise correlation of these factors with developmental fate of 6*bcd* embryos has yet to be determined.

How does expansion repair occur?

Cell death is a likely mechanism for repair of expanded domains. 6*bcd* embryos displayed increased levels of cell death

in the expanded presumptive head region, while 1*bcd* embryos had increased cell death in the abdominal segments. Wild-type embryos require cell death for normal development. A deletion mutant that eliminates *reaper*, dramatically reduces the amount of cell death throughout the embryo and shows defects in head involution and over population of the CNS and PNS (White et al., 1994). The process of head involution appears to be dependent on cell death as evidenced by the mutation *head involution defective*, which also shows reduced levels of apoptosis (Grether et al., 1995). Indeed, the expanded head regions of 4*bcd* and 6*bcd* embryos show increased *reaper* expression. Therefore excess cells in the expanded head can be eliminated and proper head involution can take place. However, there is a threshold in the number of cells that can be eliminated. Almost half of all 6*bcd* embryos had some abnormality in the head cuticular structures indicating defects in head involution. Transmitted light movies showed that one third of 6*bcd* embryos recorded died with the inability to involute head tissue or because the excess tissue prevented proper gut formation. These embryos initiate retraction of the clypeolabrum, but fail to complete head involution. In both situations, embryos were unable to remove sufficient amounts of tissue by apoptosis. If the fate map expansion is too great, errors in morphogenesis will occur. We have shown that both the salivary gland and the brain cell number is normalized in 4*bcd* and 6*bcd* embryos as well as the epidermis in 1*bcd* embryos. This analysis shows that apoptosis plays a major role in tailoring tissue to its wild-type cell number.

A possible model for *Drosophila* embryonic pattern repair

Time-lapse recordings of cell death in wild-type embryos revealed that most embryonic tissues display some level of apoptosis during development. This, we believe, indicates that most embryonic tissues are initially established with an excess of cells. Once the correct arrangement of cells is established, the excess cells die by apoptosis. Varying the maternal *bcd* dosage leads to two types of mispatterning: fate map expansion and compression. Repair of expanded regions occurs by apoptosis of the excess cells. The additional cell deaths occur on the same schedule as seen in wild-type embryos. There is an upper limit to the extent of fate map expansion that an embryo can tolerate, which was seen as either tumorous structures or epithelial breaches, which were caused by too many cells dying in a concentrated area. There are numerous examples in mammalian development of cell death eliminating excess cells after a structure is formed. The best example is in neuronal development where a large number of neurons send axons to form a particular contact; once one of the axons makes contact, the unsuccessful neurons die by apoptosis (Raff et al., 1993; Truman et al., 1992). In *Drosophila*, the final step in eye development is the removal of excess cells after ommatidia formation. This cell death is required in order to generate the near crystalline array of ommatidia (Cagan and Ready, 1989; Wolff and Ready, 1991).

Compressed regions of the embryo showed a reduction in cell death. The compressed abdominal epidermis of 6*bcd* embryos showed less apoptosis than wild-type embryos indicating that the cell number had dropped below the lower limit of cells required to properly form an epidermal segment. Similarly, the salivary gland anlage in 1*bcd* embryos may have fallen below the threshold and formed a reduced-sized salivary gland. The developing brains of 1*bcd* embryos display a reduced, but still substantial, level of cell death indicating that the embryonic brain is supplied with a greater relative excess of cells for brain development than the epidermis and salivary glands. Understanding the mechanisms that control embryonic cell death will provide information about embryonic pattern repair.

The first two authors contributed equally to this work and should be considered as first authors. We would like to thank Chuck Ettensohn and Javier López for critical reading of this manuscript. We would also like to thank the members of the Minden and Lopez labs for helpful discussions. J. M. would like to thank Bruce Alberts in whose laboratory this work was initiated and Christiane Nüsslein-Volhard for suggesting the project. T. P. was supported in part by an NSF graduate training grant to the Science Technology Center for Light Microscope Imaging and Biotechnology, BIR 9256343. J. M. is a Lucille P. Markey Scholar, and this work was supported in part by grants from the Lucille P. Markey Charitable Trust and NIH grant HD31642.

REFERENCES

Berleth, T., Burri, M., Thoma, G., Bopp, D., Richstein, S., Frigerio, G., Noll, M. and Nüsslein-Volhard, C. (1988). The role of localization of *bicoid* RNA in organizing the anterior pattern of the *Drosophila* embryo. *EMBO J.* **7**, 1749-1756.

Bomze, H. M. and López, A. J. (1994). Evolutionary conservation of the structure and expression of alternatively spliced *ultrabithorax* isoforms from *Drosophila*. *Genetics* **136**, 965-977.

Bownes, M. (1975). Adult deficiencies and duplication of head and thoracic structures resulting from microcautery of blastoderm stage *Drosophila* embryos. *J. Embryol. Exp. Morph.* **34**, 33-54.

Busturia, A. and Lawrence, P. A. (1994). Regulation of cell number in *Drosophila*. *Nature* **370**, 561-563.

Bryant, S. V., French, V. and Bryant, P. J. (1981). Distal regeneration and symmetry. *Science* **212**, 993-1002.

Cagan, R. L. amd Ready, D. F. (1989). The emergence of order in the *Drosophila* pupal retina. *Dev. Biol.* **136**, 346-262.

Cohen, S. M. and Jürgens, G. (1990). Mediation of *Drosophila* head development by gap-like segmentation genes. *Nature* **346**, 482-485.

Davidson, E. H. (1989). Lineage-specific gene expression and the regulative capacities of the sea urchin embryo: a proposed mechanism. *Development* **105**, 421-45.

DiNardo, S., Kuner, J. M., Thies, J. and O'Farrell, P. H. (1985). Development of embryonic pattern in *D. melanogaster* as revealed by accumulation of the nuclear *engrailed* protein. *Cell* **40**, 56-69.

Dohrmann, C., Azpiazu, N. and Frasch, M. (1990). A new *Drosophila* homeo box gene is expressed in mesodermal precursor cells of distinct muscles during embryogenesis. *Genes Dev.* **4**, 2098-2111.

Driever, W. and Nüsslein-Volhard, C. (1988). The BICOID protein determines position in the *Drosophila* embryos in a concentration-dependent manner. *Cell* **54**, 95-104.

Eldon, E. D. and Pirrotta, V. (1991). Interactions of the *Drosophila* gap gene *giant* with maternal and zygotic pattern-forming genes. *Development* **111**, 367-378.

Ettensohn, C. E., Malinda, K. M., Miller, R. N. and Ruffin, S. W. (1996). Cell interactions in the sea urchin embryo. *Advances in Developmental Biochem.* **4**, 47-97.

Foe, V. E. and Odell, G. M. (1989). Mitotic domains partition fly embryos, reflecting early biological consequences of determination in progress. *American Zoologist.* **29**, 617-652.

Frasch, M., Hoey, T., Rushlow, C., Doyle, H. and Levine, M. (1987). Characterization and localization of the EVEN-SKIPPED protein of *Drosophila*. *EMBO J.* **6**, 749-759.

French, V., Bryant, S. V. and Bryant, P. J. (1976). Pattern regulation in epimorphic fields. *Science* **193**, 969-981.

Frohnhöfer, H. G. and Nüsslein-Volhard, C. (1986). Organization of anterior pattern in the *Drosophila* embryo by the maternal gene *bicoid*. *Nature* **324**, 120-125.

Grether, M. E., Abrams, J. M., Agapite, J., White, K. and Steller, H. (1995).

The *head involution defective* gene of *Drosophila melanogaster* functions in programmed cell death. *Genes Dev.* **9**, 1694-1708.

Kam, Z., Minden, J. S., Agard, D. A., Sedat, J. W. and Leptin, M (1991). *Drosophila* gastrulation: analysis of cell shape changes in living embryos by three-dimensional fluorescence microscopy. *Development* **112**, 365-370.

King, B. H. and Bryant, P. J. (1982). Developmental responses of the *Drosophila melanogaster* embryo to localized X irradiation. *Rad. Res.* **89**, 590-606.

Kraut, R. and Levine, M. (1991). Spatial regulation of the gap gene *giant* during *Drosophila* development. *Development* **111**, 601-609.

Lamka, M. L., Boulet, A. M. and Sakonju, S. (1992). Ectopic expression of UBX and ABD-B proteins during *Drosophila* embryogenesis: competition, not a functional hierarchy, explains phenotypic suppression. *Development* **116**, 841-854.

Maggert, K., Levine, M. and Frasch, M. (1995). The somatic-visceral subdivision of the embryonic mesoderm is initiated by dorsal gradient thresholds in *Drosophila*. *Development* **121**, 2107-2116.

Minden, J. S. (1996). Synthesis of a new substrate for detection of *lacZ* gene expression in live *Drosophila* embryos. *BioTechniques* **20**, 122-129.

Minden, J. S., Agard, D. A., Sedat, J. W. and Alberts, B. M. (1989). Direct cell lineage analysis in *Drosophila melanogaster* by time-lapse, three-dimensional optical microscopy in living embryos. *J. Cell Biol.* **109**, 505-516.

Raff, M. C., Barres, B. A., Burne, J. F., Coles, H. S., Ishizaki, Y. and Jacobson, M. D. (1993). Programmed cell death and the control of cell survival: Lessons from the nervous system. *Science* **262**, 695-700.

Robinow, S. and White, K. (1991). Characterization and spatial distribution of ELAV protein during *Drosophila Melanogaster* development. *J. Neurobiol.* **22**, 443-461.

Rykowski, M. C. (1991). Optical sectioning and three-dimensional reconstruction of diploid and polytene nuclei. *Methods Cell Biol.* **35**, 253-286.

Schubiger, G. (1976). Adult differentiation and partial *Drosophila* embryos after ligation during stages of nuclear multiplication and cellular blastoderm. *Dev. Biol.* **50**, 476-488.

Skeath, J. B. and Carroll, S. (1992). Regulation of proneural gene expression and cell fate during neuroblast segregation in the *Drosophila* embryo. *Development* **114**, 939-946.

Struhl, G. (1989). Differing strategies for organizing anterior body pattern in *Drosophila* embryos. *Nature* **338**, 741-744.

Struhl, G., Struhl, K. and Macdonald, P. M. (1989). The gradient morphogen *bicoid* is a concentration-dependent transcriptional activator. *Cell* **57**, 1259-1273.

Tautz, D., Lehmann, R., Schnurch, H., Schuh, R., Seifert, E., Keinlin, A., Jones, K. and Jäckle, J. (1987). Finger protein of novel structure encoded by *hunchback*, a second member of the gap class of *Drosophila* segmentation genes. *Nature* **327**, 383-389.

Tautz, D. and Pfeifle, C. (1989). A non-radioactive in situ hybridization method for the localization of specific RNAs in *Drosophila* embryos reveals translational control of the segmentation gene *hunchback*. *Chromosoma* **98**, 81-85.

Truman, J. W., Thorn, R. S. and Robinow, S. (1992). Programmed neuronal death in insect development. *J. Neurobiol.* **23**, 1295-1311.

Warn, R. M. and Magrath, R. (1986). Observations by novel method of surface changes during the syncytial blastoderm stage of the *Drosophila* embryo. *Dev. Biol.* **89**, 540-548.

White, K., Grether, M. E., Abrams, J. A., Young, L., Farrell, K. and Steller, H. (1994). Genetic control of programmed cell death in *Drosophila*. *Science* **264**, 677-683.

Wolff, T. and Ready, D. F. (1991). Cell death in normal and rough eye mutants of *Drosophila*. *Development* **113**, 825-839.

(Accepted 23 January 1997)